Cellular Uptake of Elastic Nanoparticles

Xin Yi, Xinghua Shi, and Huajian Gao*

School of Engineering, Brown University, Providence, Rhode Island 02912, USA

(Received 28 July 2010; published 22 August 2011)

A fundamental understanding of cell-nanomaterial interaction is of essential importance to nanomedicine and safe applications of nanotechnology. Here we investigate the adhesive wrapping of a soft elastic vesicle by a lipid membrane. We show that there exist a maximum of five distinct wrapping phases based on the stability of full wrapping, partial wrapping, and no wrapping states. The wrapping phases depend on the vesicle size, adhesion energy, surface tension of membrane, and bending rigidity ratio between vesicle and membrane. These results are of immediate interest to the study of vesicular transport and endocytosis or phagocytosis of elastic particles into cells.

DOI: 10.1103/PhysRevLett.107.098101 PACS numbers: 87.16.D−, 46.70.Hg, 87.17.Aa, 87.17.Rt

Although rapid progress has been made in understanding the effects of size and shape on particle uptake into cells [1,2], relatively little is known about the corresponding effect of particle elasticity. Recent experiments have provided mounting evidence of the importance of elastic deformation in cellular uptake of nanoparticles. For example, it has been found that macrophages are unable to phagocytose very soft targets, which has profound implications on the functioning of the immune system [3]. Flexible erythrocytes can be strongly distorted during phagocytosis due to strong interactions between cell membrane and soft particles or vesicles [4]. Beningo and Wang [5] have shown that phagocytosis of soft microparticles can be hindered by particle deformation. Murine leukemia virus (MLV) and human immunodeficiency virus (HIV) particles regulate their mechanical properties at different stages of the life cycle through internal morphological reorganization [6]: Immature HIV viral particles are relatively stiff for budding out of a host while mature HIV particles are substantially softer for entry into a host [6]. Flexible micelles can circulate for prolonged periods in the blood stream due to their flexible structures, allowing them to deliver drugs to target tumor cells more efficiently [7]. In drug delivery, softer, more flexible particles are expected to inhibit phagocytosis, leading to a longer lifetime of particles in the circulation. Although the detailed mechanisms of cellular uptake remain to be fully elucidated and can vary in different cases, a general fact has been established that cellular uptake of nanoparticles is strongly influenced by their elastic properties. This calls for studies aimed at understanding the effect of elastic deformation of particles on cellular uptake.

Here we present the first theoretical model on the adhesive wrapping of an elastic, deformable vesicle by a lipid membrane, for a range of bending rigidity ratio between the vesicle and membrane. Using theoretical analysis and molecular simulations we will show how the wrapping degree depends on the vesicle size, the adhesion energy, the surface tension of the membrane, and the bending rigidity ratio. We will determine the phase diagrams for cellular uptake of three-dimensional axisymmetric (3D) and two-dimensional (2D) particles, probing the transitions between full wrapping, partial wrapping, and no wrapping states. We will also discuss possible implications of our results on relevant biological processes.

Note that there can be a number of alternative models for an elastic particle. Here we model the engulfed particle as an elastic vesicle with a constant total surface area A_t. Consider such a vesicle wrapped by an initially flat membrane with elastic deformation in both the vesicle and the membrane, as shown in Fig. 1(a). The total energy of the system can be described by the Canham-Helfrich Hamiltonian as [8–11]

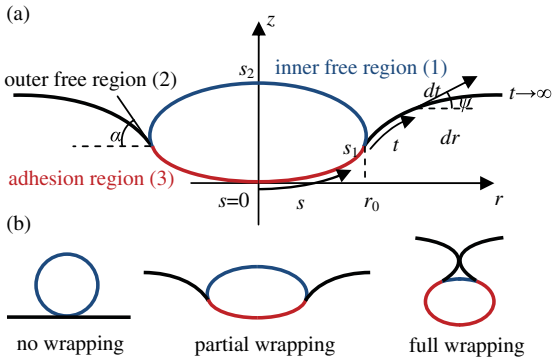

FIG. 1 (color online). Schematic of an elastic vesicle wrapped by an initially flat membrane. (a) The geometry of the system with wrapping angle α and tangent angle ψ. Arclengths s and t are defined along the vesicle and along the outer free part of the membrane, measured from the bottom pole ($s = 0$) and the adhesion edge $t = 0$ ($s = s_1$), respectively; r_0 is the $r(s)$ coordinate at $s = s_1$. (b) Schematic of the three characteristic wrapping states. No wrapping is the state with zero contact area. Full wrapping is the state in which the left and right sides of the membrane touch each other on the top of the vesicle. Partial wrapping corresponds to the intermediate scenario with incomplete wrapping.

$$E = \sum_{i=1,2,3} \int (2\kappa_i M^2 + \kappa_i^g G) dA_i + \Delta P V + \sigma \Delta A - \gamma A_3 + \Gamma A_t, \quad (1)$$

where M is the mean curvature, G is the Gaussian curvature, κ_i and κ_i^g are the bending and Gaussian moduli of the three regions, respectively; $\Delta P = P_{\text{out}} - P_{\text{in}}$ is the pressure difference between the outside and inside of the vesicle; V is the volume of the vesicle; σ is the surface tension of the membrane which is conjugated with the excess area ΔA induced by wrapping; γ is the specific adhesion energy; and A_3 is the contact area. The last term arises from the constraint that the surface area A_t is fixed, Γ being the Lagrange multiplier. Although not considered in our model, a spontaneous curvature can be readily included in the formulation. Hereafter we use subscripts 1, 2, and 3 to identify quantities associated with the inner free, outer free, and the wrapped regions, respectively. To simplify our description, we assume that the Gaussian modulus of the adhesion region is $\kappa_3^g = \kappa_1^g + \kappa_2^g$, which implies that the Gaussian curvature does not affect the vesicle shape due to the Gauss-Bonnet theorem [12]. We will further assume $\kappa_3 = \kappa_1 + \kappa_2$ throughout the analysis, while recognizing important exceptions such as the formation of clathrin or caveolin coats during the wrapping process. All length scales are scaled by the effective radius of the vesicle $a = \sqrt{A_t/(4\pi)}$. In two dimensions, the vesicle length L_t remains constant and the effective radius is $a = L_t/(2\pi)$. Other dimensionless parameters are $\bar{\gamma} = 2\gamma a^2/\kappa_2$, $\bar{\sigma} = 2\sigma a^2/\kappa_2$, $\eta = 2\Gamma a^2/\kappa_2$, and $p = \Delta P a^3/\kappa_1$.

The axisymmetric shapes in Fig. 1(a) are determined from the tangent angle $\psi(s)$ with geometric relations $\dot{r} = \cos\psi$ and $\dot{z} = \sin\psi$, where dots denote derivatives with respect to the rescaled arclength s of the vesicle or to arclength t of the outer free part of the membrane. For the axisymmetric configuration, variation of the energy functional in Eq. (1) gives rise to the following governing equation for the vesicle shape

$$\ddot{\psi} = -\frac{\dot{\psi}^2 \tan\psi}{2} - \frac{\dot{\psi}\cos\psi}{r} + \frac{\cos^2\psi + 1}{2r^2}\tan\psi + \frac{\kappa_2}{2\kappa_i}(\eta + \bar{\sigma} - \bar{\gamma})\tan\psi + \frac{\kappa_1}{2\kappa_i}\frac{pr}{\cos\psi} \quad (2)$$

for the wrapped region of the vesicle. The same equation with $\bar{\sigma}$ and $\bar{\gamma}$ removed would hold for the inner free region of the vesicle [13]. The equations that govern the shape of the outer free part of the membrane can be found in Ref. [11] and are listed in the Supplemental Information [14] for the convenience of the reader. For the two-dimensional configuration, the corresponding shape equations of the vesicle are $\kappa_i\ddot{\psi}/\kappa_1 = \mu\sin\psi + pr\cos\psi$ $(i = 1, 3)$ and $\dot{\mu} = p\sin\psi$ [10], and the shape equation of the outer free membrane is $\ddot{\psi} = \bar{\sigma}\sin\psi/2$ [15]. The boundary conditions are $\psi_3(0) = 0$ and $r_3(0) = 0$ at $s = 0$, and $\psi_1(s_2) = \pi$ and $r_1(s_2) = 0$ at $s = s_2$. The remote boundary conditions are $\lim_{t\to\infty}\psi_2(t) = 0$ and $\lim_{t\to\infty}\dot{\psi}_2(t) = 0$ as $t \to \infty$, which enforce the asymptotic flatness of the membrane at large distances [11]. At the adhesion edge $s = s_1$, the radial coordinate r and tangent angle ψ must be continuous, and the variation of energy E yields the following boundary conditions:

$$\begin{aligned} \kappa_1\dot{\psi}_1^2 + \kappa_2\dot{\psi}_2^2 - \kappa_3\dot{\psi}_3^2 &= 2\gamma a^2, \\ \kappa_1\dot{\psi}_1 + \kappa_2\dot{\psi}_2 - \kappa_3\dot{\psi}_3 &= 0, \end{aligned} \quad (3)$$

which represent the balance of tangential force and torque at $s = s_1$ [16]. Equation (3) reduces to $\dot{\psi}_2(s_1) = \dot{\psi}_3(s_1)$ and $\dot{\psi}_1(s_1) - \dot{\psi}_2(s_1) = \sqrt{2\gamma a^2/\kappa_1}$ in the limit $\kappa_2 \to \infty$, which coincides with the corresponding condition for a vesicle on a flat or curved rigid substrate [10,17] or a rigid particle wrapped by a lipid membrane [11,18]. In addition, the condition for the balance of normal force at $s = s_1$ is [16]

$$\kappa_1\ddot{\psi}_1 + \kappa_2\ddot{\psi}_2 - \kappa_3\ddot{\psi}_3 = 0. \quad (4)$$

The equilibrium configurations of the vesicle and membrane can be found numerically by solving Eq. (2) with continuity and boundary conditions in Eqs. (3) and (4). These boundary conditions are only valid in the equilibrium state. To calculate the energy at any given value of the wrapping degree $f = A_3/A_t$ which may not be in equilibrium, the balance equations (3) and (4) do not hold. In that case we vary the values of $r_0 (\in [0, s_1])$ and α with a step size 0.0005 in r_0 and 0.001 in α for a given f, obtain solutions by the shooting method and then determine the shapes of the vesicle and membrane from solution with the lowest energy. An equilibrium state corresponds to a local extremum of free energy as f increases from 0 to 1. Numerical results show that the boundary conditions in Eqs. (3) and (4) are indeed satisfied in equilibrium states [14]. The effect of pressure difference on the wrapping phases is rather minor in 2D and negligible in 3D [14], and is therefore neglected in the following analysis. A similar method has been used to study the axisymmetric equilibrium shapes of erythrocytes considering vesicle-vesicle adhesion [19].

We now investigate the effects of bending modulus ratio κ_1/κ_2 and normalized adhesion energy $\bar{\gamma}$ on the stability of different wrapping states. Figure 2 shows the energy change $\Delta E = E - E_0$ as a function of the wrapping degree f, where E_0 is the ground state energy taken as $8\pi\kappa_1$ for a spherical vesicle and $\pi\kappa_1/a$ for a circular vesicle. Figure 2(a) shows that there exist three phases in 2D. For relatively small adhesion energy, the bending energy dominates the wrapping process and full wrapping cannot happen. As $\bar{\gamma}$ increases, the stable wrapping state changes from no wrapping to partial wrapping then to full wrapping. For $\bar{\gamma} = 10$, the global minimum is $f = 1$ for $\kappa_1/\kappa_2 \geq 1$ and $f < 1$ for $\kappa_1/\kappa_2 = 0.1$. This means that larger adhesion energy is needed for a softer vesicle to be

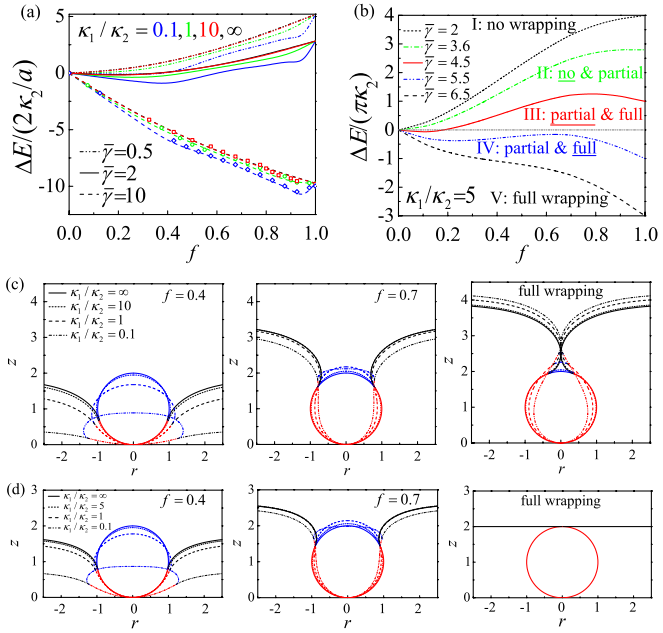

FIG. 2 (color online). Energy change ΔE as a membrane wraps around a particle with wrapping degree f for different $\bar{\gamma}$ and κ_1/κ_2 with $\bar{\sigma} = 1$. (a) Two-dimensional case, and (b) three-dimensional case. Scatters in (a) are results from molecular simulations [14]. In general, there exist 5 distinct wrapping phases in 3D. Plots shown in (b) show that, under the selected parameters, there are 2 stable (I, V) and 3 metastable phases (II–IV). Among the 3 metastable phases, the underlined wrapping states in (b) are the ones with lower energy. (c) 2D and (d) 3D solutions to selective wrapping configurations at $\bar{\sigma} = 2$ for different particle-membrane rigidity ratios κ_1/κ_2.

fully engulfed. Compared to the 2D case, the axisymmetric configuration exhibits five possible phases (I–V) as introduced in Ref. [11] [see Fig. 2(b)]. In phase I, $\bar{\gamma}$ is low and ΔE increases monotonically with f. As $\bar{\gamma}$ increases, there exists a stable state (no wrapping) and a metastable partial wrapping state and phase II arises. Further increase of $\bar{\gamma}$ results in a global minimum at a partial wrapping state with an energy barrier to reach the metastable full wrapping state (phase III). With increasing $\bar{\gamma}$ the stable partial wrapping state becomes metastable with respect to a stable full wrapping state (phase IV). If $\bar{\gamma}$ is large enough, the energy barrier vanishes and the full wrapping state becomes the only stable state in phase V. For each phase, there is a stable state (global energy minimum) and possibly a metastable state (local energy minimum). For very soft particles (e.g., $\kappa_1/\kappa_2 < 1$), the phase II′ no longer has no wrapping as the stable state and partial wrapping as a metastable state; instead the no wrapping state becomes unstable while partial wrapping becomes stable. There are three cases of possible energy evolution profiles as a function of the wrapping degree. Case 1 exhibits a global energy minimum at a relatively small f and possibly a metastable state at a relatively large f; case 2 shows a global minimum at a relatively large f and a possible metastable state at a relatively small f; case 3 has only one global minimum at large f [14]. The boundaries between these cases correspond to the thin (dash-dotted and solid) lines in Figs. 3(d) and 3(e). Figures 2(c) and 2(d) show sequences of vesicle-membrane configurations in 2D and 3D at $\bar{\sigma} = 2$ for different rigidity ratios κ_1/κ_2.

With the knowledge of energy functions for κ_1/κ_2, $\bar{\sigma}$, and $\bar{\gamma}$, the phase diagrams of wrapping have been calculated and shown in Fig. 3. Note that the solution at $f = 1$ is unphysical since in that case two opposing parts of the membrane on top of the particle will have crossed each other. Therefore, the state of full wrapping needs to be carefully defined [Fig. 1(b)]. In the 2D case, the shape equation for the outer free part of the membrane associated with a given wrapping angle α can be derived analytically as $\psi_2 = 4\arctan[\tan\frac{\alpha}{4}\exp(-t\sqrt{\bar{\sigma}/2})]$, where t is the rescaled arclength of the outer free part [15]. With the relation $\dot{r} = \cos\psi$, the $r(t)$ coordinate can be determined as

$$r(t) = r_0 + t + \sqrt{\frac{2}{\bar{\sigma}}}\frac{(1 - e^{\sqrt{2\bar{\sigma}}t})(1 - \cos\alpha)}{1 - \cos\frac{\alpha}{2} + e^{\sqrt{2\bar{\sigma}}t}(1 + \cos\frac{\alpha}{2})}. \quad (5)$$

For a given set of r_0, α, and $\bar{\sigma}$, the minimum of $r(t)$ can be determined. The full wrapping condition is found from the condition that the minimum of $r(t)$ is equal to zero as shown in Fig. 3(a). The critical condition for a rigid circular particle to be fully wrapped by a membrane is then given by [18]

$$\sqrt{\frac{\bar{\sigma}}{2}}\sin\alpha = \sqrt{2} - 2\cos\frac{\alpha}{2} + \ln\left(\tan\frac{\pi}{8}\right) - \ln\left(\tan\frac{\alpha}{4}\right), \quad (6)$$

with $\alpha = \arccos[1 - (1 - \sqrt{\bar{\gamma}})^2/\bar{\sigma}]$. The derivation of Eq. (6) is based on the assumption that the full wrapping state is a stationary state with zero slope along the energy evolution curve as a function of wrapping degree, which is true for large κ_1/κ_2 or small κ_1/κ_2 with large $\bar{\sigma}$. For small κ_1/κ_2 with small $\bar{\sigma}$, the full wrapping state has the lowest energy but the corresponding slope of the energy profile does not vanish [14]. Figure 3(a) shows that a minimum adhesion energy $\bar{\gamma}_{\min}$ is necessary for partial wrapping. The softer the vesicle is, the smaller $\bar{\gamma}_{\min}$ is. For a rigid circular particle, $\bar{\gamma}_{\min} = 1$ [18]. As κ_1/κ_2 decreases, $\bar{\gamma}$ needs to increase to maintain the full wrapping state. When $\bar{\sigma} \leq 0.5$, there are small differences between the transition lines from the state of partial wrapping to full wrapping for different κ_1/κ_2. As $\bar{\sigma}$ increases, the differences become large and strikingly sensitive to κ_1/κ_2.

Since there is no analytical expression for $r(t)$ in the 3D case, we take $f = 1$ as the full wrapping condition for simplicity. For a rigid spherical particle, $\bar{\gamma}_{\min} = 4$ [11]. There is no phase II for $\kappa_1/\kappa_2 = 1$ and 0.1 since the adhesion energy can compensate for the bending energy at the initial wrapping process for small κ_1/κ_2 [Figs. 3(d) and 3(e)]. The effects of κ_1/κ_2 on the phase transition are

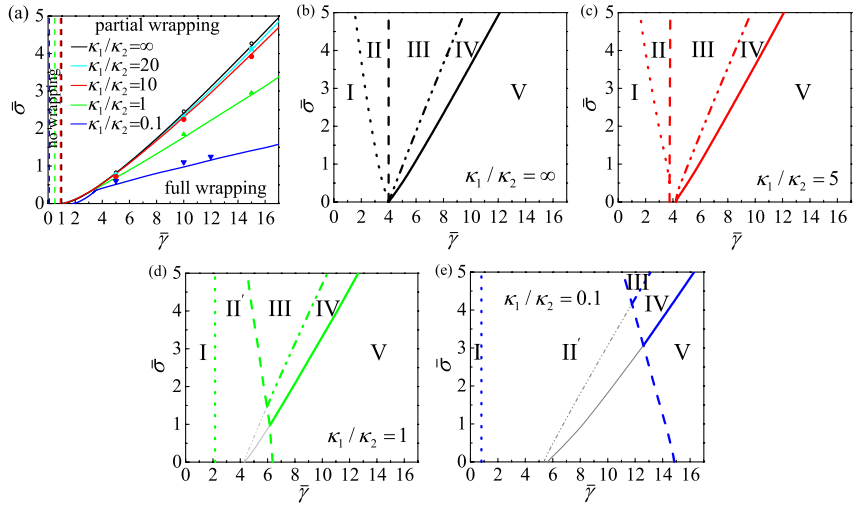

FIG. 3 (color online). Wrapping phase diagrams with respect to normalized adhesion energy $\bar{\gamma}$ and surface tension $\bar{\sigma}$ at different values of the rigidity ratio κ_1/κ_2. (a) 2D case, dashed lines: boundaries between no wrapping and partial wrapping states, solid lines: boundaries between partial and full wrapping states. (b)–(e) 3D cases for $\kappa_1/\kappa_2 = \infty$, 5, 1, 0.1, dotted lines: boundaries between phases I and II(II′), dashed lines: boundaries between phases II(II′) and III(III–V for $\kappa_1/\kappa_2 = 1$, 0.1), dash-dotted lines: boundaries between phases III and IV, solid lines: boundaries between phases IV and V. Symbols in (a) denoting transition boundaries between the partial and full wrapping states are from molecular simulations [14].

very small when $\kappa_1/\kappa_2 \geq 1$ but large for very soft vesicles ($\kappa_1/\kappa_2 = 0.1$). A general result from Fig. 3 is that stiffer particles require lower adhesion energy for wrapping. Comparison with Fig. 3(a) indicates that $\bar{\gamma}_{\min}$ is larger in 3D than in 2D for a given κ_1/κ_2, since the bending energy density is larger in 3D. For a given κ_1/κ_2, the critical value of $\bar{\gamma}$ for full wrapping is larger in 3D when $\bar{\sigma}$ is small ($\bar{\sigma} < 1$ for $\kappa_1/\kappa_2 \geq 1$, $\bar{\sigma} < 0.5$ for $\kappa_1/\kappa_2 = 0.1$). When $\bar{\sigma}$ exceeds a certain value, the critical value of $\bar{\gamma}$ for full wrapping in 3D becomes smaller, indicating that the uptake of a two-dimensional particle could not be accomplished even if full wrapping becomes possible in three dimension. In such cases, spherical particles can be absorbed when cylindrical ones cannot.

The phase diagrams shown in Fig. 3 may have broad implications for endocytosis or phagocytosis and drug or gene delivery processes. If the adhesive interaction between a particle and membrane is not strong enough, it will be difficult for the cell membrane to engulf a very soft particle. To achieve the full wrapping state and engulf the particle, the bending modulus of the particle needs to increase. Protein coating formation and actin polymerization beneath the membrane are effective methods to increase bending modulus of the particle. For example, binding of clathrin-associated proteins leads to a significant increase in the rigidity of clathrin-coated vesicles which is about 20 times that of the vesicle membrane alone [20]. For streptavidin- and avidin-coated vesicles $\kappa_1 \approx 320 k_B T$ and $\kappa_1 \approx 115 k_B T$, respectively, which are much larger than bare SOPC/capBio-DOPE vesicles with $\kappa_1 \approx 10 k_B T$ [21]. The actin concentration inside the phagocytic cup has been estimated to increase the local stiffness by a factor of 5 [22]. The phase diagrams in Fig. 3 provide a possible alternative view on why clathrin and other protein coatings as well as actin polymerization are involved in many endocytosis and phagocytosis processes.

Macrophages have a preference to engulf rigid targets with more actin filaments concentrated beneath stiffer particles [5]. In some cases, infected macrophages are drug targets; while in other cases, macrophages are not target cells but act as barriers by phagocytosis preventing particles from releasing their therapeutic cargos near or within target cells [23]. Figure 3 demonstrates that uses of soft particles and cylindrical particles can postpone or prevent uptake. An alternative method is to increase the bending modulus of the cell membrane. For three-dimensional particles, the effects of particle elasticity on cellular uptake are only evident when $\kappa_1 < \kappa_2$. Wormlike viruses and particles with very high aspect ratios [2] may be considered two-dimensional vesicles. For these types of particles, controlling the particle stiffness can be essential for controlling cellular uptake. Many particles can be used as soft drug delivery particles such as polymer particles, nanocapsules, and nanogel with high water content. The elasticity- and geometry-induced inhibition of cellular uptake will have important applications in the use of those particles as drug delivery carriers.

Experiments show that MLV and HIV particles are stiff during viral budding out of the host and soften during entry activities [6]. For these viral particles, entry into the cell often involves endocytosis and membrane fusion, in which case full wrapping is not necessary for the uptake process. In contrast, the budding process involves no membrane fusion and requires full wrapping, so that the stiffness of

the particle can be expected to play a more important role. However, softer particles experience smaller energy changes during the wrapping process [see Fig. 2(a) for 2D cases] which might be preferred in case full wrapping is not required. These results provide feasible explanations why viral particles harden right before budding and then soften again in the uptake stage [6].

Our analysis suggests that the reason why soft particles are less prone to wrapping than stiff ones could be understood as follows. For a rigid particle, the adhesive interaction between the particle and membrane simply forces the membrane to deform and wrap around the particle. In contrast, Figs. 2(c) and 2(d) show that for a soft particle, the deformation is partitioned between the particle and the membrane at different stages of wrapping. A very soft particle would initially spread along the membrane without significant membrane deformation. Only at a later stage will the membrane be forced to bend around the particle. Thus, wrapping around a rigid particle involves a gentler rise in elastic energy in the membrane as more membrane area deforms around the particle. When wrapping around a soft particle, the membrane does not deform initially but then needs to catch up to almost the same configuration at full wrapping. This means a more abrupt rise in elastic energy at the later stage of wrapping and, consequently, larger adhesion energy would be required to balance the more rapid rise in elastic energy. Since it is this partition of deformation at the early stage of wrapping that hinders the full wrapping of a soft particle, alternative particle models, such as a particle with a bulk elastic modulus or a thin shell with shear rigidity, are not expected to change this basic feature of particle-membrane interaction. Therefore, we believe the conclusions of our study should be generic and not specific to the present vesicle model.

In this Letter, we have performed both theoretical analysis and molecular simulations to study the cellular uptake of elastic nanoparticles. Using variational methods and free energy functional for cell membrane wrapping around elastic cylindrical (2D) or spherical particles (3D), we have calculated the associated phase diagrams describing transition boundaries between different wrapping phases. We find that stiffer particles can achieve full wrapping more easily than softer particles, while softer particles experience smaller energy changes during wrapping and might be more favorable in case full wrapping is not necessary. The cellular uptake of particles is strongly dependent on the particle size, shape, and physicochemical properties of particles [1,2,24]. Our results suggest that precise control of the particle elasticity can be another appealing way to control cellular uptake. The present model can be extended to problems such as phase separations and assembly of programmable soft materials.

Support from the National Science Foundation (Grant No. CMMI-1028530), and the KIMM-Brown I-CTC project is gratefully acknowledged.

*huajian_gao@brown.edu

[1] M. P. Desai *et al.*, Pharm. Res. **14**, 1568 (1997); H. Gao, W. Shi, and L. B. Freund, Proc. Natl. Acad. Sci. U.S.A. **102**, 9469 (2005).
[2] J. A. Champion and S. Mitragotri, Proc. Natl. Acad. Sci. U.S.A. **103**, 4930 (2006).
[3] S. L. Tao and T. A. Desai, J. Control. Release **109**, 127 (2005).
[4] J. A. Swanson and A. D. Hoppe, J. Leukoc. Biol. **76**, 1093 (2004).
[5] K. A. Beningo and Y. L. Wang, J. Cell Sci. **115**, 849 (2002).
[6] N. Kol *et al.*, Biophys. J. **91**, 767 (2006); N. Kol *et al.*, Biophys. J. **92**, 1777 (2007).
[7] Y. Geng *et al.*, Nature Nanotech. **2**, 249 (2007).
[8] W. Helfrich, Z. Naturforsch. C **28**, 693 (1973).
[9] F. Jülicher and R. Lipowsky, Phys. Rev. Lett. **70**, 2964 (1993).
[10] U. Seifert and R. Lipowsky, Phys. Rev. A **42**, 4768 (1990); U. Seifert, Phys. Rev. A **43**, 6803 (1991).
[11] M. Deserno, Phys. Rev. E **69**, 031903 (2004).
[12] E. Kreyszig, *Differential Geometry* (Dover Publications, Mineola, New York, 1991).
[13] F. Jülicher and U. Seifert, Phys. Rev. E **49**, 4728 (1994).
[14] See Supplemental Material at http://link.aps.org/supplemental/10.1103/PhysRevLett.107.098101 for the governing equations of the membrane wrapping problem, several supplemental figures from numerical calculations, and details of molecular simulations.
[15] M. M. Müller, M. Deserno, and J. Guven, Phys. Rev. E **76**, 011921 (2007).
[16] M. Deserno, M. M. Müller, and J. Guven, Phys. Rev. E **76**, 011605 (2007); J.-B. Fournier, Soft Matter **3**, 883 (2007).
[17] S. Das and Q. Du, Phys. Rev. E **77**, 011907 (2008).
[18] S. A. Nowak and T. Chou, Phys. Rev. E **78**, 021908 (2008).
[19] J. Derganc *et al.*, Biophys. J. **84**, 1486 (2003).
[20] A. L. Jin *et al.*, Biophys. J. **90**, 3333 (2006).
[21] S. Dieluweit *et al.*, Langmuir **26**, 11041 (2010).
[22] J. S. van Zon *et al.*, Mol. Syst. Biol. **5**, 298 (2009).
[23] S. M. Moghimi, A. C. Hunter, and J. C. Murray, Pharmacol. Rev. **53**, 283 (2001).
[24] N. A. Licata and A. V. Tkachenko, Phys. Rev. Lett. **100**, 158102 (2008).

Supplementary Information for "Cellular Uptake of Elastic Nanoparticles"

Xin Yi, Xinghua Shi, and Huajian Gao

School of Engineering, Brown University, Providence, Rhode Island 02912, USA

I. NUMERICAL RESULTS IN THE 2D CASE

Fig. S1 shows the energy change as a lipid membrane wraps around a 2D circular particle with wrapping degree f for different $\bar{\gamma}$ with very small $\bar{\sigma}$ ($p = 0$, $\kappa_1/\kappa_2 = 0.1$, $\bar{\sigma} = 0.15$). When $\bar{\sigma}$ is very small, a coexistence of the partial and full wrapping states emerges, corresponding to two local energy minima. The wrapping states with lower energy in the coexistence regions are underlined. For $\bar{\gamma} = 3$ the full wrapping state marked by the open square arises before the wrapping fraction f reaches the position marked by the solid circle; in other word, the solution at the solid point is unphysical in this case.

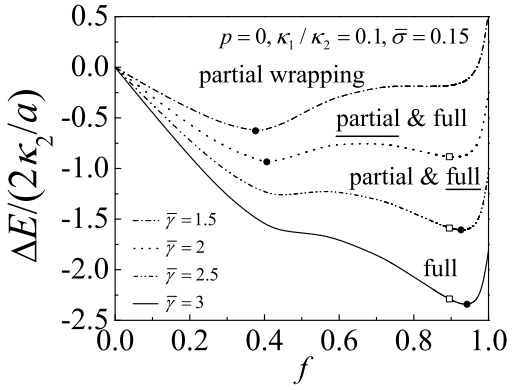

FIG. S1: Energy change ΔE as a function of the wrapping degree f for different $\bar{\gamma}$ with $p = 0$, $\kappa_1/\kappa_2 = 0.1$ and $\bar{\sigma} = 0.15$. The solid circle on each curve corresponds to the global minimum. The open squares correspond to the full wrapping states. The underlined wrapping states are the ones with lower energy.

Fig. S2(a) shows a zoom of the $\bar{\sigma} \leq 0.5$ part of the phase diagram Fig. 3(a) in the main text. As $\bar{\sigma}$ becomes very small, a coexistence of the partial and full wrapping states emerges for particles with $\kappa_1 = 0.1\kappa_2$, as shown in Fig. S1. Since the size of nanoparticles engulfed by cells is usually smaller than a few hundred nanometers and the pressure difference ΔP is of the order of $1\mathrm{N/m}^2$, we take $p = \pm 2$ as examples to investigate the contribution of pressure difference to the wrapping phase diagrams. Compared with the phase diagram with $p = 0$ (see Fig. 3(a)), the boundaries between partial and full wrapping states for $\kappa_1/\kappa_2 = 20, 10, 1, 0.1$ are slightly higher at $p = -2$ (see Fig. S2(b)), and slightly lower at $p = 2$ (see Fig. S2(d)). In the region for small $\bar{\sigma}$, the partial and full wrapping states coexist only for $\kappa_1/\kappa_2 = 0.1$ at $p = -2$ (see Fig. S2(c)), but for both $\kappa_1/\kappa_2 = 1$ and 0.1

at $p = 2$ (see Fig. S2(e) and (f)). Comparison of the 2D phase diagrams at different values of p indicates a finite but minor effect of pressure difference on nanoparticle uptake.

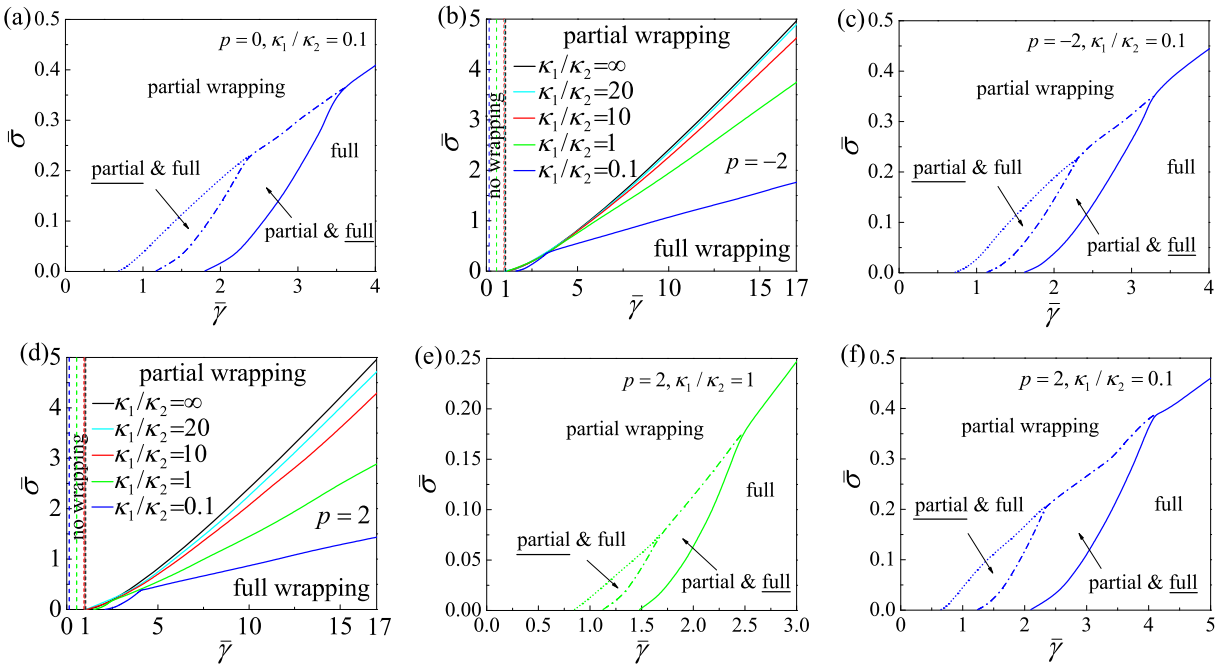

FIG. S2: Wrapping phase diagrams with respect to normalized adhesion constant $\bar{\gamma}$ and surface tension $\bar{\sigma}$ at different values of the rigidity ratio κ_1/κ_2 in the 2D case. (a) A zoom on the region for small values of $\bar{\sigma}$ with the normalized pressure difference $p = 0$ and the rigidity ratio $\kappa_1/\kappa_2 = 0.1$ in Fig. 3(a) of the main text; (b) phase diagram with $p = -2$; (c) a zoom of the small $\bar{\sigma}$ part of the phase diagram in (b); (d) phase diagram with $p = 2$; (e),(f) zooms of the small $\bar{\sigma}$ parts of the phase diagram in (d) with $\kappa_1/\kappa_2 = 1$ and 0.1, respectively. The underlined wrapping states are the ones with lower energy.

Fig. S3 shows how the local geometric properties (such as the distance to symmetry axis r_0, the wrapping angle α, the curvatures $\dot{\psi}_1(s_1)$, $\dot{\psi}_2(0)$ and $\dot{\psi}_3(s_1)$, and $\ddot{\psi}_1(s_1)$, $\ddot{\psi}_2(0)$ and $\ddot{\psi}_3(s_1)$; see Fig. 1) and wrapping fraction evolve as $\bar{\sigma}$ changes for $\bar{\gamma} = 10$ at the adhesion edge $s = s_1$. For rigid particles, we have $1 + \sqrt{2\bar{\sigma}} \sin\frac{\alpha}{2} = \sqrt{\bar{\gamma}}$, $r_0 = \sin\alpha$, $f = \alpha/\pi$, $\dot{\psi}_1 = \dot{\psi}_3 = 1$, $\dot{\psi}_2(t = 0) = -\sqrt{2\bar{\sigma}} \sin\frac{\alpha}{2} = 1 - \sqrt{\bar{\gamma}}$, $\ddot{\psi}_1 = \ddot{\psi}_3 = 0$, and $\ddot{\psi}_2(t = 0) = \frac{\bar{\sigma}}{2} \sin\alpha$. For elastic particles, there are no analytical solutions. Numerical results show that in elastic cases r_0 increases, and α and $f(s_1)$ decrease with increasing $\bar{\sigma}$, which has the same trend as the rigid case (see Fig. S3(a-c)). Due to the deformation of the circular particle, the local curvatures at $s = s_1$ are no longer constant. As $\bar{\sigma}$ increases, curvatures $\dot{\psi}_1(s_1)$, $\dot{\psi}_2(0)$ and $\dot{\psi}_3(s_1)$ decrease (see Fig. S3(d-f)). The softer the particle is, the larger the deformation is and the more deviation would be from the rigid case. These results confirm that the contact boundary conditions in Eqs. (3-4) are indeed satisfied.

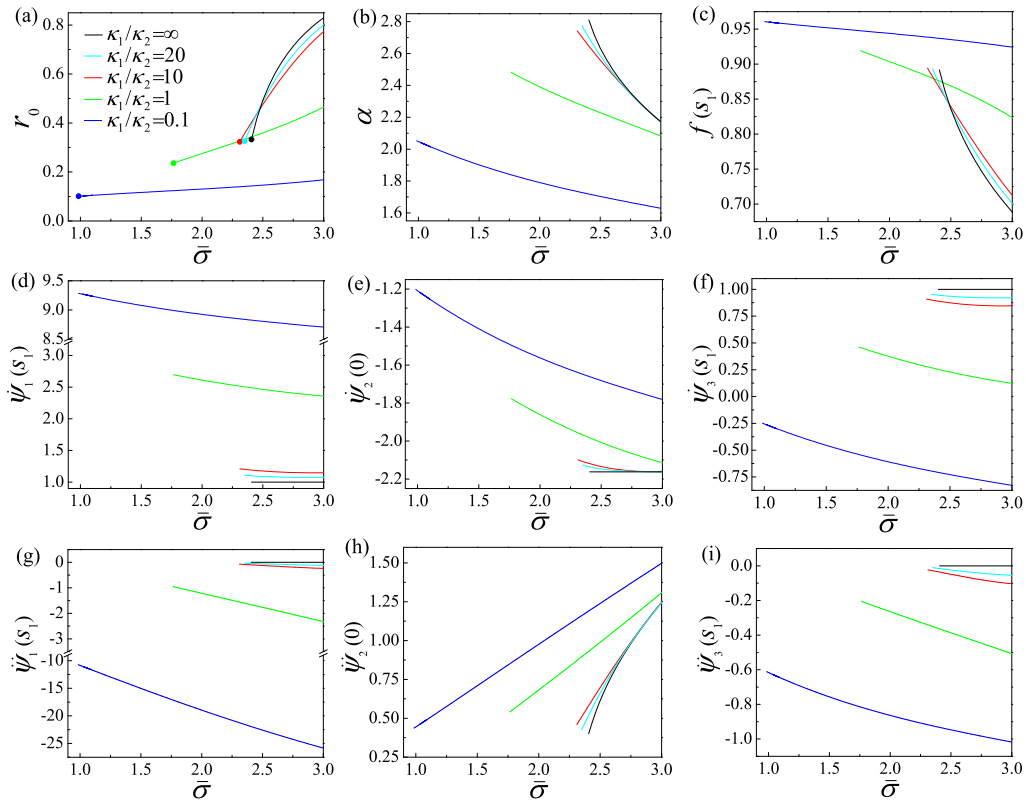

FIG. S3: (a) The distance to symmetry axis r_0 of the adhesion edge $s = s_1$, (b) the wrapping angle α, (c) the wrapping fraction $f(s_1) = s_1/\pi$, (d),(e),(f) the contact curvatures and (g),(h),(i) $\ddot{\psi}_1$, $\ddot{\psi}_2$ and $\ddot{\psi}_3$ at $s = s_1$ of the inner free, outer free and adhesion regions, respectively, as functions of $\bar{\sigma}$ for different rigidity ratios κ_1/κ_2 at $\bar{\gamma} = 10$. The solid circle on each curve in (a) corresponds to the full wrapping state which persists for even smaller $\bar{\sigma}$. The lines have been colored according to the conventions defined in (a).

II. NUMERICAL RESULTS IN THE 3D CASE

The governing equation for the vesicle shape is Eq. (2) in the main text. The equations that govern the shape of the outer free part of the membrane can be found in Ref. [1] and are listed here as

$$\begin{cases} \ddot{\psi} = \dfrac{1}{r}\left(\dfrac{\sin\psi}{r}\cos\psi + \dfrac{\bar{\sigma}r}{2}\sin\psi - \dot{\psi}\cos\psi + \dfrac{\mu}{2}\sin\psi\right), \\ \dot{\mu} = \dot{\psi}^2 - \dfrac{\sin^2\psi}{r^2} + \bar{\sigma}(1-\cos\psi), \\ \dot{r} = \cos\psi, \end{cases}$$

where dots denote derivatives with respect to the rescaled arclength of the outer free part of the membrane.

Fig. S4 shows typical energy landscapes of the three cases in phase II′ for several values of $\bar{\gamma}$. In case 3 the energy change between the global minimum and the full wrapping state ($f = 1$) is about $4k_BT$ with $\kappa_2 = 20k_BT$, and might be overcome by thermal fluctuations. This indicates that the thin solid line in Fig. 3(e) can be viewed as the transition line between phase II′ and phase V approximately.

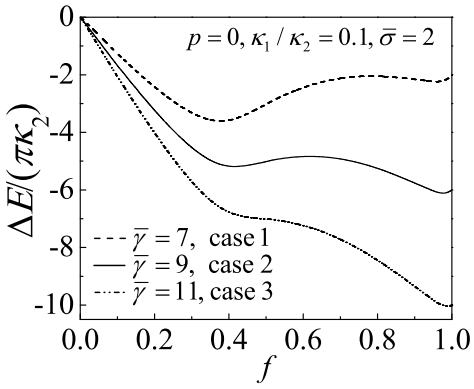

FIG. S4: Energy changes ΔE of the three cases in phase II′ as a function of the wrapping degree f for different $\bar{\gamma}$ ($p=0$, $\kappa_1/\kappa_2=0.1$ and $\bar{\sigma}=2$).

Fig. S5 (a) is a combination plot of the phase diagrams in Fig. 3(b-e) in which the phase boundary difference is shown. Wrapping phase diagrams at $p=\pm 2$ are shown in Fig. S5(a) and (b). There is very small difference between these three phase diagrams, indicating a negligible contribution of pressure difference to phase diagrams.

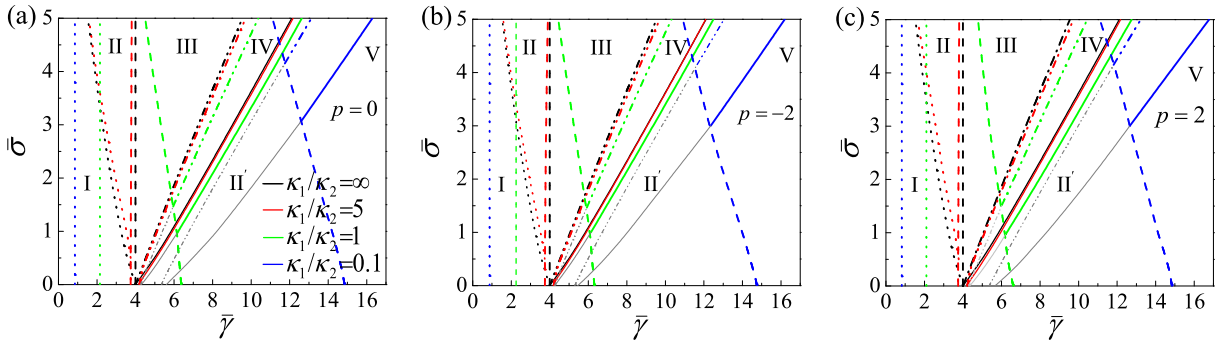

FIG. S5: Wrapping phase diagrams with respect to normalized adhesion constant $\bar{\gamma}$ and surface tension $\bar{\sigma}$ at different values of the rigidity ratio κ_1/κ_2 in the 3D case with normalized pressures $p=0,-2,2$ in (a), (b) and (c), respectively. The definitions of phases I-V and II′ are in main text. The lines have been colored according to the conventions defined in (a).

Fig. S6 shows the evolution of geometric properties and wrapping fraction of the global minimum states for different κ_1/κ_2. For rigid particles $\dot{\psi}_1=\dot{\psi}_3=1$, $\dot{\psi}_2(t=0)=1-\sqrt{\bar{\gamma}}$, $\ddot{\psi}_1=\ddot{\psi}_3=0$ and r_0, α, $f(s_1)$ and $\ddot{\psi}_2(t=0)$ can be determined numerically. When $\bar{\sigma}$ decreases from 5 to the values marked by the solid circles, the global minimum states transfer from the partial wrapping states to full wrapping states ($f=1$), and stay at $f=1$ as $\bar{\sigma}$ decreases. Results in Fig. S6 confirm that the boundary conditions in Eqs. (3-4) are indeed satisfied.

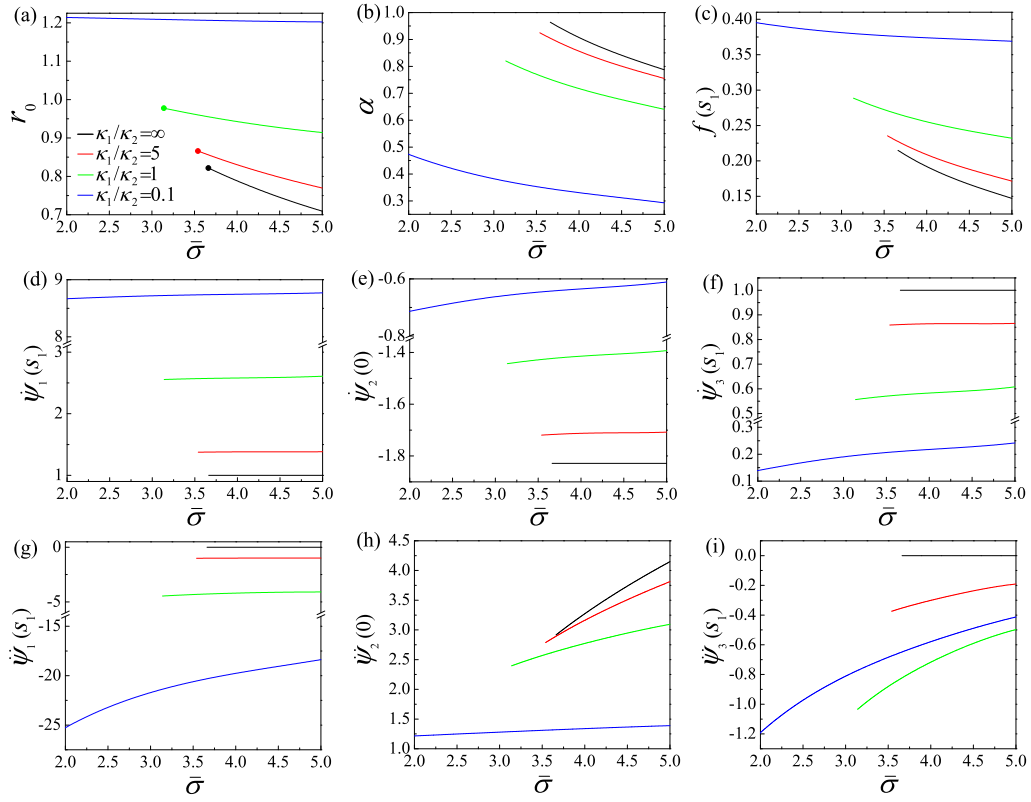

FIG. S6: (a) The distance to symmetry axis r_0 of the adhesion edge $s = s_1$, (b) the wrapping angle α, (c) the wrapping fraction $f(s_1)$, (d),(e),(f) the contact curvatures, and (g),(h),(i) $\ddot{\psi}_1$, $\ddot{\psi}_2$ and $\ddot{\psi}_3$ at $s = s_1$ of the inner free, outer free and adhesion regions, respectively, as functions of $\bar{\sigma}$ for different rigidity ratios κ_1/κ_2 at $\bar{\gamma} = 8$. The lines have been colored according to the conventions defined in (a).

III. MOLECULAR SIMULATIONS IN THE 2D CASE

In two dimensions the Canham-Helfrich Hamiltonian reduces to $E = \sum_{i=1,2,3} \int u_i dA_i + \Delta PV + \sigma\Delta A - \gamma A_3$, where $u_i = \kappa_i C^2/2$ $(i = 1, 2, 3)$ are the bending energy densities of the membrane regions depending on C, the local curvature of the membrane. Based on the elastic thin shell theory, the bending energy density of a thin shell in two-dimensional deformation is $u = DC^2/2$, where $D = Eh^3/[12(1-\nu^2)]$ is the bending stiffness, E, ν and h are the Young's modulus, Poisson's ratio and thickness of the shell, respectively [2]. Comparing it with the Helfrich energy, we have a correspondence $\kappa \to D$, which enables us to model a circular vesicle and the membrane as isotropic inextensible elastica in molecular simulations.

To simulate the wrapping of a particle in two dimensions (2D), we adopt a coarse grained simulation scheme in which a one-layer-thick cylindrical shell and a one-layer-thick membrane are constructed. In this system, the particles formed the shell and membrane are modeled by 3-body potential of Tersoff's form, with parameters from Refs. [3,4]. The interaction between particles of shell and membrane is described by the Lennard-Jones

potential $4\varepsilon\left[\left(\frac{\sigma}{r}\right)^{12}-\left(\frac{\sigma}{r}\right)^{6}\right]$, where r is the distance of two particles, σ is the distance at which the potential is zero and ε is the depth of the potential well. Driven by the adhesion energy, the membrane can wrap around the shell. In such a manner, the simulation system can explicitly depict all the energy components of elastic cylindrical shell-membrane system. For example, the total elastic energy of the modeled membrane is composed of in-plane stretching energy and bending energy, similar to that of the cell membrane. In the simulations, periodic boundary conditions are imposed in the axial direction of the shell during the wrapping process. For simplicity, temperature is fixed at 1K in all simulations to eliminate the thermal effect. The rigidity of the shell can be adjusted by the parameter of the Tersoff potential. The specific interaction energy γ and the bending modulus κ_1, κ_2 are obtained with the methods described in Refs. [5,6].

---

[1] M. Deserno. Elastic deformation of a fluid membrane upon colloid binding. Phys. Rev. E **69**, 031903 (2004).

[2] S. P. Timoshenko and J. M. Gere, *Theory of Elastic Stability*, 2nd Ed., (McGraw-Hill, New York, 1961).

[3] S. J. Stuart, A. B. Tutein and J. A. Harrison. A reactive potential for hydrocarbons with intermolecular interactions. J. Chem. Phys. **112**, 6472 (2000).

[4] D. W. Brenner, O. A. Shenderova, J. A. Harrison, S. J. Stuart, B. Ni and S. B. Sinnott. A second-generation reactive empirical bond order (REBO) potential energy expression for hydrocarbons. J. Phys.: Condens. Matter **14**, 783 (2002).

[5] X. Shi, N. M. Pugno and H. Gao. Tunable core size of carbon nanoscrolls. J. Comput. Theor. Nanosci. **7**, 517 (2010).

[6] X. Shi, Y. Cheng, N. M. Pugno and H. Gao. Tunable water channels with carbon nanoscrolls. Small **6**, 739 (2010).